NASA TM X- 66182

PRIMARY COSMIC RAY ELECTRONS ABOVE 10 GeV- EVIDENCE FOR A SPECTRAL BREAK

ROBERT F. SILVERBERG

JONATHAN F. ORMES

V. K. BALASUBRAHMANYAN

JANUARY 1973

GSFC —— **GODDARD SPACE FLIGHT CENTER**
GREENBELT, MARYLAND

PRIMARY COSMIC RAY ELECTRONS ABOVE 10 GeV -

EVIDENCE FOR A SPECTRAL BREAK

ROBERT F. SILVERBERG
JONATHAN F. ORMES
V. K. BALASUBRAHMANYAN

$\mathcal{I}$

PRIMARY COSMIC RAY ELECTRONS ABOVE 10 GeV - EVIDENCE FOR A SPECTRAL BREAK

by

Robert F. Silverberg‡
Jonathan F. Ormes
V. K. Balasubrahmanyan

NASA/Goddard Space Flight Center
Greenbelt, Maryland 20771

ABSTRACT

A balloon borne measurement of the cosmic ray electron spectrum from 10 to 200 GeV is reported in which two new techniques have been used to remove proton background contamination. First, the depth of the spectrometer was more than 25 radiation lengths, the equivalent of more than 2 mean free paths of material, enabling hadronically and electromagnetically induced cascades to be differentiated for a subset of the data. Second, electromagnetic cascade starting points were determined to within ± 0.1 radiation lengths based upon a calibration with electrons from 5.4 to 18 GeV at the Stanford Linear Accelerator, greatly reducing the chances for a proton to simulate an electron. The resulting spectrum, when fitted with a power law, is quite steep, -3.2 ± 0.1, but the chi-square fit is marginal. A significantly better fit is achieved assuming a transition region model in which the source spectral index is 2.7 with a break occurring at about 50 GeV.

Introduction

The energy spectrum of primary cosmic electrons above 1 GeV has
been given much attention in recent years because the electrons represent
an important probe into the history and structure of the galaxy. They
may provide information on the origin of all cosmic rays and on the back-
ground of electromagnetic radiation. The electron spectrum is expected
to exhibit a steepening at an energy related to the photon and magnetic
energy density in the interstellar region where electrons are stored.

While results up to several hundred GeV have been obtained in balloon
flights, [Nishimura et al., 1969, Anand et al., 1968, 1969, Scheepmaker,
1971, Meyer and Müller, 1971] serious discrepancies in the spectral shape
and absolute intensity are apparent, and hence it is difficult to arrive
at specific conclusions about the electron propagation.

In the hope of clarifying the experimental situation, a large area
detector was developed for use in a series of balloon flights. The ex-
periment worked well on flights 1 and 3 which were flown from Alamogordo,
New Mexico on April 28, 1969, at 7.9 g/cm^2 residual atmosphere and on
November 11, 1970 at 7.4 g/cm^2. A total exposure factor of ≈ 4000 M^2-ster-sec
was obtained. The experiment provided very detailed information on each
event. Twenty three detectors were used to identify each event and sample
the longitudinal electromagnetic cascade development. Each of these de-
tectors was pulse height analyzed over a dynamic range of 10^4. A digital
spark chamber provided trajectory data for each particle. Data on the
primary cosmic ray proton and helium spectrum using this instrument has
previously been published [Ryan et al., 1972].

DESCRIPTION OF THE DETECTOR

A diagram of the detector as flown on flight 3 is shown in figure 1. It consists of three sections: a section for particle identification, an electromagnetic shower section, and a nuclear cascade section. The charge module is made up of four detectors; two 1/4" plastic scintillators, a 1/2" acrylic plastic Cerenkov detector, and a 1/8" cesium iodide scintillator. Each of these detectors is viewed by photomultipliers and their outputs are pulse height analyzed. Included in the charge module also is a digital spark chamber of the type developed by Ehrmann et al., [1967]. This chamber allows particle trajectories to be determined so that geometrical corrections can be made to the pulse heights from the large area detectors. The spark chamber is also very useful in eliminating background particles entering the sides of the detector which satisfy the trigger criteria.

The electromagnetic shower section of the experiment is composed of twelve modules, each of which consists of a 1/8" thick tungsten sheet and 1/4" plastic scintillator representing 0.9 radiation lengths. Each module is viewed by two photomultiplier tubes whose outputs are summed and pulse height analyzed.

Although the nuclear cascade section was primarily for measurement of the high energy proton spectrum, it was extremely useful for determining the interacting proton background correction to the electron intensity. The nuclear cascade section consists of seven iron modules, each one about 4.5 radiation lengths thick [0.5 nuclear mean free paths]. Again a sandwich structure is employed by alternating layers of plastic scintillators

and iron. Each iron module contains three plastic scintillators viewed by two photomultipliers tubes whose outputs are summed and pulse height analyzed.

TRIGGERING MODES OF THE EXPERIMENT

In order to reduce background and the dead time in the experiment, the electron trigger criteria were set to demand the equivalent of a 7 GeV electron in the tungsten modules. In addition a minimum pulse height was demanded in each of the 12 tungsten modules which required that the cascades develop very rapidly. This not only discriminated against low energy particles, but also eliminated triggers from high energy protons interacting deep in the tungsten. The only protons which triggered the experiment in the electron mode were those which interacted early enough in the tungsten stack to deposit a large energy in all the tungsten modules.

Two other important modes were included in the experiments: these are the proton and calibration modes. In the proton trigger mode, a particle must deposit greater than 40 GeV in the nuclear cascade section of the experiment. Events were allowed to trigger in both the electron and proton modes simultaneously. These events were used to understand interacting proton background as discussed later. The calibration mode permits any charged particle which passed through both of the plastic scintillators in the charge module to trigger the experiment. This mode is used on the ground for calibration of individual detector elements on sea level muons. During the 1970 flight, every 32nd event opened a gate which permitted a calibration mode event to be recorded. In this way detector performance was monitored during the flight.

CALIBRATION OF THE EXPERIMENT

While the instrument provides a great deal of information about each
particle which triggers it, the transition effect [Pinkau, 1965] and the
lack of any simple and reliable approximation to showers in heavy mater-
ials make interpretation of the data difficult. It was realized early
in the detector development that calibration of the instrument would be
mandatory.

The detector was calibrated on positrons from 5.4 to 18 GeV at the
Stanford Linear Accelerator, SLAC, in 1969. The mean energy deposition
for various energies and angles of incidence was normalized in terms of
the energy deposition due to sea level muons which could penetrate the
85 gm/cm^2 of the detector. All of these were then fitted to the expressions

$$f\ (E_O,t_O,t)=\exp\ (at+bt^2)\quad t\leq\alpha+0.5 \tag{1}$$

$$f\ (E_O,t_O,t)= [\frac{y-0.56}{t(t-\alpha)}]^{1/2}\ \exp\ \{-t+2\ [(t-\alpha)\ (y-0.56)]^{1/2}\}\quad t>\alpha+0.5 \tag{2}$$

where $f\ (E_O,t_O,t)$ is the energy deposition that an electromagnetic cascade
initiated by an electron of energy E_O will produce at depth t, if it
started to cascade at depth t_O. The variables y and t are related to
the incident energy and the depth by

$$y=\ln\ (\frac{E_O}{E_C}),\ and\ t=\frac{SD+t_O}{\cos\theta}$$

respectively where S is the detector module number, D is the depth in
radiation lengths of one tungsten module, and θ is the angle of incidence
with respect to the normal. $E_C, D, t_O,$ and α are free parameters which are
determined by simultaneously fitting the observed showers at eight dif-
ferent energies to equations 1 and 2, [see Crannell et al., 1972 for a
discussion of the calibration procedures]. The parameters a and b are
uniquely determined by requiring $f\ (E_O,t_O,t)$ and its first derivatives to

be continuous at $t=\alpha+0.5$. Equation (2) is after Heisenberg [1946] and

is based on approximation A of cascade theory. Equation (1) is simply

used to carry the Heisenberg expression below the singularity at $t=\alpha$.

Knowing E_c, D, and the energy deposition of an electron of unknown

energy impinging on the instrument, the data from an event can be fitted

to the electromagnetic cascade curves to determine an "apparent starting

point" of the shower, t_o, and the incident energy, E_o.

These parameters are determined by the minimization of

$$\chi^2 = \sum_{i=1}^{12} \left\{ \frac{f(E_o,t_o,t_i)}{\sigma(E_o,t_o,t_i)} - f_i \right\}^2 \tag{3}$$

where $\sigma^2(E_o,t_o,t_i)$ is the variance of $f(E_o,t_o,t_i)$. At SLAC energies,

we observed $\sigma^2(E_o,t_o,t_i) \approx f(E_o,t_o,t_i)$ except at small depths where the

deviations were larger. χ^2 also gives a measure of the likelihood of

the incident particle being an electron and the data from SLAC provides

a χ^2 distribution for electrons to compare against flight particles.

Note that equation (3) represents a fit with 10 degrees of freedom so

that E_o and t_o are well determined.

The energy distribution observed by applying the procedure outlined

above to a run with 18 GeV electrons from SLAC is shown in Figure 2. The

FWHM of the distribution is ~17%. The small peak below 40 GeV is due to

two 18 GeV electrons incident on the experiment within the resolving time

of the experiment [a frequent occurrence at SLAC, but not a problem in

flight].

DISCRIMINATION AGAINST PROTONS

Since the electron component of cosmic rays is at best only a few

percent of the proton component, the most serious problem in measuring

electrons is to reduce to a negligible contribution those interacting protons which may masquerade as electrons. Nuclear interactions which produce a π^0 meson may produce a shower that is, in practice, indistinguishable from a shower produced by an electron.

Our study of accelerator electrons and inflight high energy protons has revealed that the method of fitting the showers to the equation above provides a sensitive means of discrimination against the proton background. In figure 3 a distribution of "apparent starting points" is presented for a sample of 16 GeV electrons from SLAC. This histogram is representative as no energy dependence was noted in the 5.4 to 18 GeV range. It should be noted that the "apparent starting point" distribution peaks at about 0.41 r. l. before the tungsten stack. This agrees quite well with 0.29 radiation lengths of material that are calculated to be in the charge module preceding the tungsten stack and suggests that this distribution's width represents real fluctuations in the production of the first high energy cascade photon.

In contrast to the electrons, a group of singly charged particles was selected from the 1970 flight which deposited >40 GeV in the iron and >5 GeV in the tungsten. The condition that the energy deposited in the iron exceed the energy deposited in the tungsten was also imposed to get a set of inflight interacting protons. Their "apparent starting point" distribution is plotted in figure 4.

The distribution in figure 4 exhibits marked structure. The source of the structure is not completely understood. One quarter of the nuclear interactions should take place in the plastic scintillators which are invisible on this radiation length scale. The structure is probably the

result of the transport of γ-rays from π⁰ decay into subsequent tungsten

slabs. However, the process of fitting electromagnetic shower curves to

nuclear interactions may shift the "apparent starting point" by a few

tenths of a radiation length. In any case, the structure is real, is

present for protons and especially for background events, and says that

the shower fitting procedure is defining an "apparent starting point"

with an accuracy of approximately 0.1 radiation length. This has the

effect of greatly reducing the amount of material in which a proton can

interact to simulate an electron.

ELECTRON SELECTION

Each possible electron event is examined to be sure that it is caused

by a singly charged particle as determined by the top plastic scintillator

and the Cerenkov detector. Both of these detectors are 30 cm above the

tungsten stack. If the particle is singly charged, the spark chamber data

is used to extrapolate the path of the particle to the twelfth tungsten

module. Only particles whose trajectories pass within the inner 80% of the

area of the 12th tungsten module are analyzed so a well defined geometry

is used for flux calculations.

Each event accepted is then fitted to the electromagnetic shower

function to determine its energy, E_O, and apparent starting point, t_O.

The minimum χ^2 is examined to see if its value is less than the 0.95

probability point for electrons of energy E_O. If it is, and if the starting

point is in the range for electrons observed at SLAC, the particle is

accepted as an electron.

RESIDUAL PROTON BACKGROUND AND OTHER CORRECTIONS

Even though unambiguous identification of each incident particle

should be attainable with nuclear emulsions, emulsion techniques are responsible for perhaps the highest [Anand et al., 1968] and the lowest [Marar et al., 1971] measured primary cosmic ray electron intensities. Other workers have used statistical separation of the protons and electrons. Scheepmaker [1971] has used the spectrum of interacting alpha particles in flight to estimate the interacting proton spectrum. Earl et al., [1972] and Meyer and Müller, [1971] have used data and extrapolations from accelerator pions and protons to determine the proton induced contamination.

The unique feature of this experiment is its total depth of four nuclear mean free paths of material. This depth allows secondaries from nuclear interactions to interact again and reveal themselves as proton induced showers.

Although our rejection of such events is still a statistical one, we can use flight data itself to determine the proton background for this experiment. A subset of the apparent electrons [those which satisfied all of the above criteria] is selected which have trajectories which pass through at least three of the seven iron modules. This subset of about 25% of the events is examined to determine the fraction which deposited significantly more energy in the iron than could be expected of an electron of energy E. This leads to a 29±5% correction which is then applied to all the data.

The final spectrum includes corrections to the data for energy loss due to bremsstrahlung in the residual atmosphere, atmospheric secondaries, spark chamber inefficiency and dead time due to paralysis of the experiment during event readout. The correction for re-entrant albedo electrons

is negligible at the energies measured.

ENERGY DEPENDENT EFFECTS

Extensive investigations for any energy dependent effect in selection were also carried out. Energy dependence due to backscatter into the spark chamber or into the charge determination section was studied by examining the data from the spark chamber and the S_2 scintillator below it, as a function of energy. No significant correlation was found between larger numbers of sparks and large pulse heights in the scintillator as a function of the estimated energy of the incident particle. No determination of any backward transport of gamma rays could be made, but the work of Ford [1972] indicates that back-scattering gamma rays greater than 2 MeV occur in less than 2% of the electron showers at high energies.

A significant energy dependence was found in the χ^2 distribution, an effect that was also observed in our positron data from SLAC. The χ^2 value below which 95% of the SLAC positrons fell was found to increase like $E^{0.31}$. The spreading of the χ^2 distribution is qualitatively in agreement with our expectation since we observed that the standard deviations in the showers were larger than expected early in the showers. As energy rises there are more data points early in the shower [relative to shower maximum] and hence our underestimation of the deviations would make the parameter χ^2 rise as a function of energy.

To further check the data for energy dependent effects, the single particle events that failed the electron selection criteria were sorted into energy bins. Their spectral index was found to be -2.7±0.2, the same as the high energy proton spectrum [Ryan et al., 1972].

The final correction for proton contamination as determined by the

spectrometer is nearly energy independent, which is surprising because
of the difference in spectra. Probably the proton rejection due to starting
point location and cascade shape is better at high energies because the
electromagnetic showers are less subject to fluctuations than their
hadronic counterparts. This proves the background rejection ratio is
improving at the same time the proton to electron ratio is going up.

Vis-a-vis other experiments, we would like to point out that a pro-
ton contamination of only 30% at low energies could become much larger
at high energies since the electron and proton spectra are not the same.

DISCUSSION

While the intensity in figure 5 agrees with the measurements of
many other workers at about 10 GeV, the spectrum is significantly steeper.
Assuming the data can be represented by a single power law over the range
10-200 GeV, the spectral index obtained is -3.2+0.1. This spectral index
is steeper than the often quoted value of ~2.7, [Bleeker et al., 1968,
Scheepmaker, 1971], although steep spectra have previously been reported
[Earl et al., 1972, Nishimura et al., 1969, Rubstov and Zatsepin, 1968,
Webber and Rockstroh, 1972].

The spectrum shows no sharp "break" but does exhibit a consistent
drop off in intensity. The Chi-square test for 8 degrees of freedom
indicates that a power law represents a marginal fit to the data (al-
most 3 standard deviations).

The spectral index is expected to steepen by a full power if
synchrotron and inverse Compton losses are dominant, based on the leakage
lifetime approximation. This approximation has, however, been called
into question by Jokipii and Meyer [1968] because it replaces the

diffusion term in the continuity equation by a characteristic loss term. Even the assumption of isotropic diffusion with a disk-shaped source region, produces a spectrum with two "breaks" each of one half a power at energies separated by a factor of 50 or more depending on the dimensions of the source region. Jokipii and Meyer predict a break in the 1-10 GeV range, but they also point out that the assumption of isotropic diffusion is probably not realistic.

Berkey and Shen [1969] have carried out a similar treatment using convection diffusion and find only one "break" occurs. However, their calculation does not include perpendicular diffusion nor the role of random magnetic field lines allowing escape from the disk. Using our data, the different models could certainly not be distinguished. A fit to a leakage lifetime model was thus attempted because of the poor fit to the power law.

From Ramaty [1972], we find that the spectral break region can be represented in the following manner. If the source spectrum is of the form $Q(E) \rightarrow E^{-\Gamma}$, then the equilibrium intensity $I(E)$, would satisfy the expression

$$I(E)E^{\Gamma} \rightarrow \int_{0}^{1/\alpha} (1-\alpha x)^{\Gamma-2} e^{-x} dx \qquad (4)$$

with $\alpha = \frac{WET}{307}$, where W is the electromagnetic energy density in eV/cm^3, and T is the mean electron lifetime in mega-years. The energy at which $\alpha=1$ is defined as the "break" energy.

The transition region model fits the data at about the 1 standard deviation level and yields a value of 2.7 for Γ, the source spectral index and a break energy of ∿50 GeV. Not too much significance should be attached to the particular model used or to the values obtained for the parameters;

the transition region model contained one more free parameter than the
power law model, and the minimum in the chi-square was very broad.

The two fits to the data are illustrated in figure 6 where $E^3 x \frac{dN}{dE}$
is plotted as a function of energy. [This representation is chosen to
emphasize details of the data]. The best power law and the transition
region model fits are indicated. The transition region model break
corresponds to a life of about 6×10^6 years assuming $W \sim 1$ eV/cm^3.

Our data argues strongly against a spectrum as hard as −2.7 around
100 GeV, and is suggestive that the data cannot be represented by a single
power law over the range 10-200 GeV. The theoretical interpretation of
this result in terms of the leakage lifetime approximation is not clear.

In view of the apparent complexity of the electron spectrum in the
high energy region, new data above 100 GeV and more precise data below
will be required to further our understanding. This is essential if
we are to answer more questions about the cosmic electrons, their
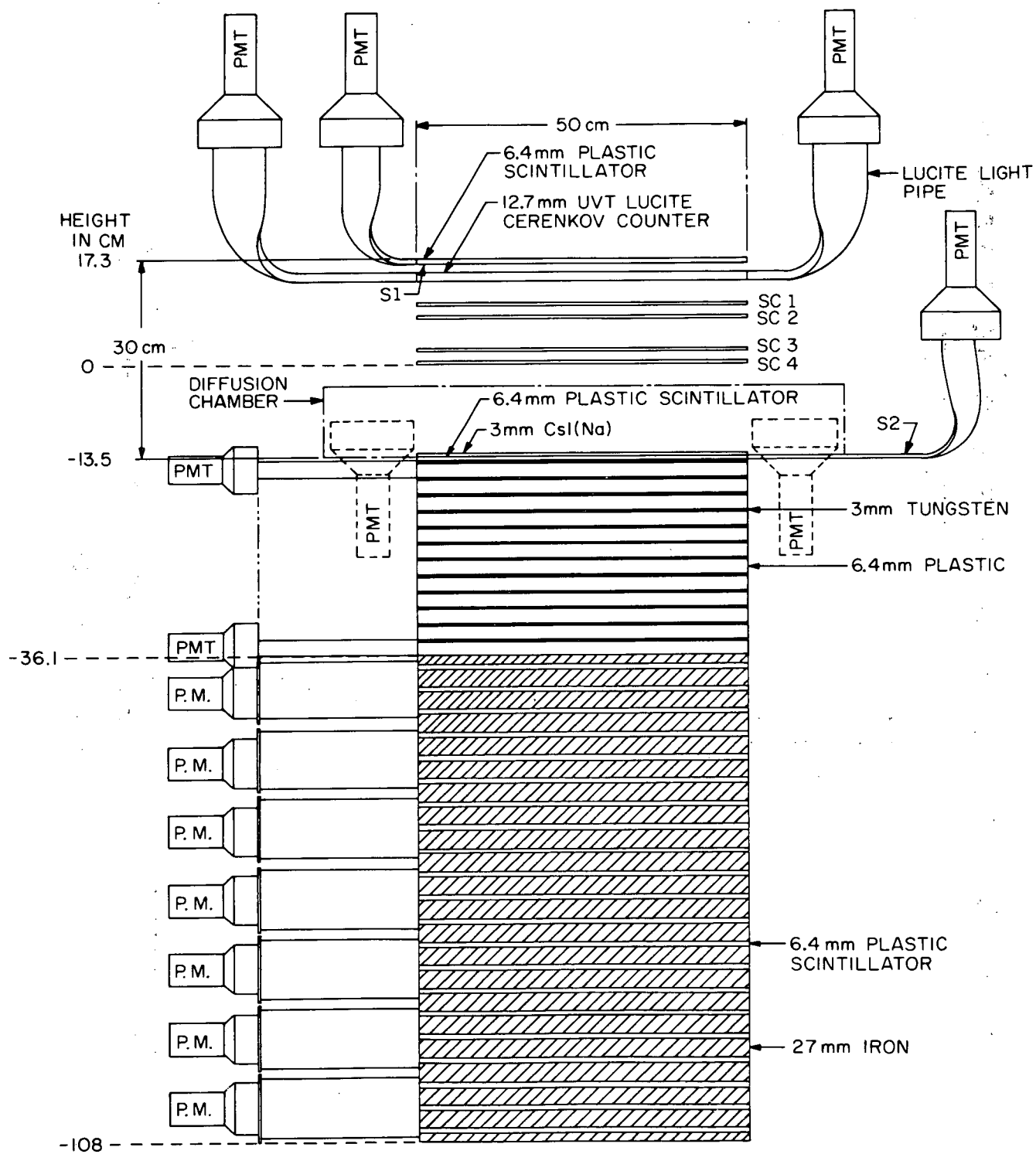sources and their propagation through the galaxy.

ACKNOWLEDGEMENTS

FIGURE CAPTIONS

Figure 1 - Diagram of the ionization spectrometer showing the physical
layout of the various component parts.

Figure 2 - Estimated energy distribution for cascades initiated by 18 GeV
electrons.

Figure 3 - "Apparent Starting Point" distribution for electromagnetic
cascades initiated by 16 GeV electrons. The origin of the
abscissa references the top of the tungsten stack.

Figure 4 - "Apparent Starting Point" distribution for singly charged
cosmic ray primaries depositing ≥ 40 GeV in iron stack and
≥ 5 GeV in tungsten stack.

Figure 5 - Differential spectrum of cosmic ray electrons (this experiment
and other workers)

Figure 6 - Differential spectrum of cosmic ray electrons at the top of
the atmosphere multiplied by E^3. The two successful flights
are shown separately along with best fits to models.

/3

REFERENCES

Anand, K. C., R. R. Daniel, and S. A. Stephens, Cosmic-ray Electron Spectrum above 50 BeV and its Implications for Cosmic-ray Confinement, Phys. Rev. Lett., 20, 764, 1968

Anand, K. C., R. R. Daniel, and S. A. Stephens, The Cosmic-ray Electron Spectrum at Energies >100 GeV, Paper presented at the XIth Int. Conf. on Cosmic Rays, Budapest, 1969

Berkey, G. B. and C. S. Shen, Origin and Propagation of Cosmic Ray Electrons, Phys. Rev., 188, 1994, 1969

Bleeker, J. A. M., J. J. Burger, A. J. M. Deerenberg, A. Scheepmaker, B. N. Swanenburg, and Y. Tanaka, Energy Spectrum of Primary Electrons in the Range 0.5 - 30 GeV, Can. J. of Physics, 46, S522, 1968

Crannell, C. J., R. A. Gearhart, F. A. Hagen, W. V. Jones, R. J. Kurz, J. F. Ormes, R. D. Price, R. F. Silverberg, and G. M. Simnett, Electron Calibration of a High-Energy Cosmic Ray Detector, Submitted to Nucl. Instr. and Methods, 1972

Daniel, R. R., and S. A. Stephen, Recent Observations on Cosmic Electrons and Their Consequences on Different Cosmic Ray Models and Related Astrophysical Quantities, Proc. Ind. Acad. Sci, 65, 319, 1967

Earl, J. A., D. E. Neally, and T. A. Rygg, Balloon Measurements of the Energy Spectrum of Cosmic Electrons Between 1 and 25 GeV, J. Geophys. Res. 77, 1087, 1972

Ehrmann, C. H., C. E. Fichtel, D. A. Kniffen and R. W. Ross, A Magnetic Core Digitized Spark Chamber for Space Science Experiments, Nucl. Instr. and Methods, 56, 109, 1967

Faneslow, J. L., R. C. Hartman, R. H. Hildebrand and P. Meyer, Charge Composition and Energy Spectrum of Primary Cosmic Ray Electrons, Astrophys. J., 158, 771, 1969

Ford, R., Private Communication, 1972

Heisenberg, W., Cosmic Radiation, Dover Publications, New York, pp. 11-25, 1946

Hovestadt, D., and P. Meyer, The Geomagnetic Cut-Off at Fort Churchill and the Primary Cosmic Ray Electron Spectrum from 10 MeV to 12 GeV in 1968, presented at the XIth Int. Conf. on Cosmic Rays, Budapest, 1969

Jokipii, J. R., and P. Meyer, Storage and Diffusion of Cosmic-Ray Electrons in the Galaxy, Phys. Rev. Letters, 20, 752, 1968
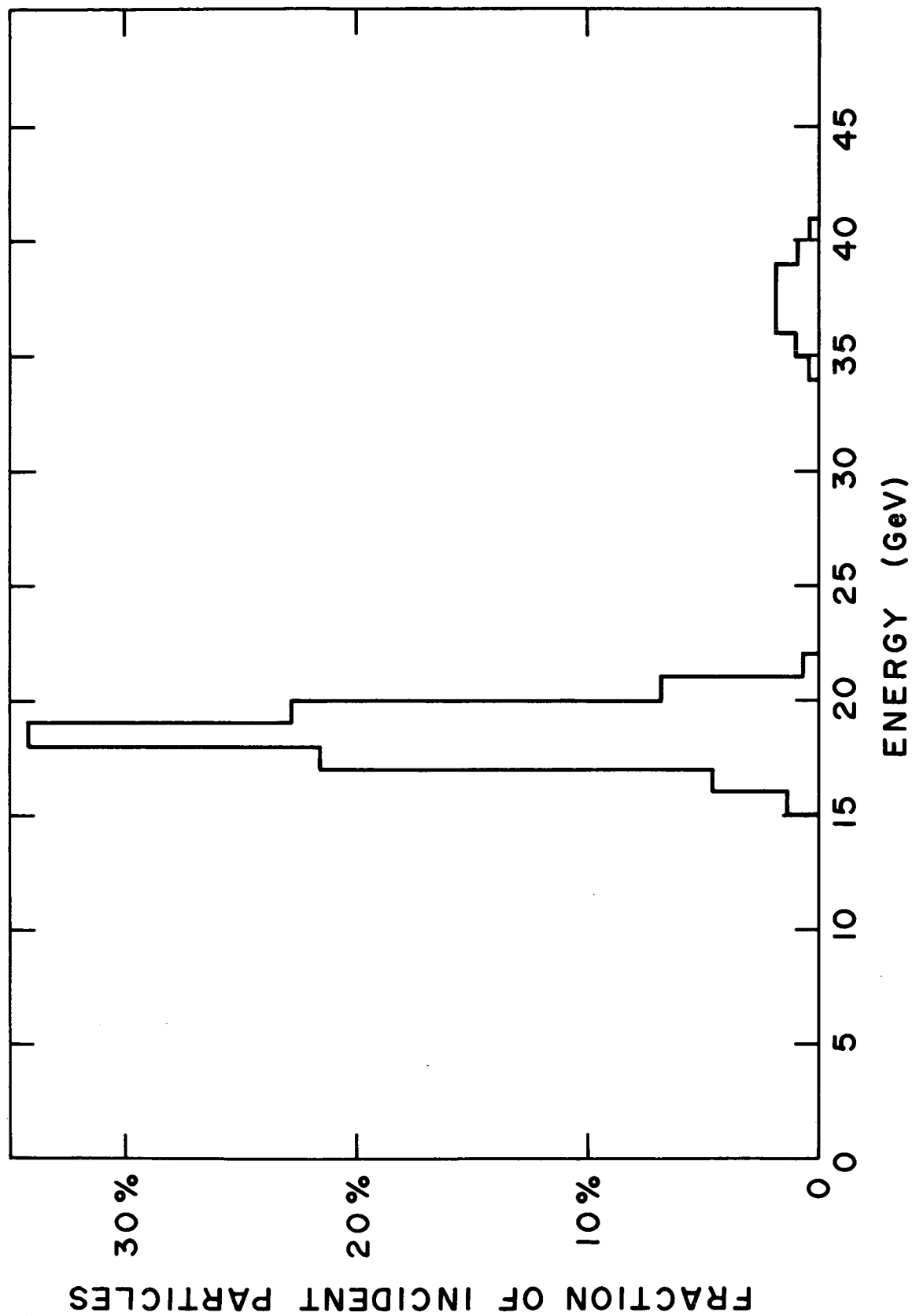
/4

REFERENCES (cont.)

Marar, T. M. K., P. S. Frier and C. J. Waddington, Intensity and
    Energy Spectrum of Energetic Cosmic Ray Electrons, J. Geophys.
    Res., 76, 1625, 1971

Meyer, P. and D. Müller, Flux and Energy Spectrum of Cosmic Ray Elec-
    trons between 10 and 1000 GeV, presented at the XIIth Int. Conf.
    on Cosmic Rays, Hobart, Tasmania, 1971

Nishimura, J., E. Mikumo, I. Mito, K. Niu, I. Ohto, and I. Tiara,
    Observation of the Electron Component in Cosmic Rays with Emulsion
    Chamber, Presented at the XIth Int. Conf. on Cosmic Rays, Budapest,
    1969

Pinkau, K., Errors in Electromagnetic Cascade Measurements due to the
    Transition Effect, Phys. Rev., 139, B1548, 1965

Ramaty, R., Private Communication, 1972

Ryan, M. J., J. F. Ormes, and V. K. Balasubrahmanyan, Cosmic Ray Pro-
    ton and Helium Spectra Above 50 GeV., Phys. Rev. Letters, 28,
    985, 1972

Rubstov, V. I., and V. I. Zatsepin, The Electron Energy Spectrum in the
    Flux of Galactic Cosmic Rays, Can. J. of Phys., 46, 518, 1968

Scheepmaker, A., Primary Cosmic Ray Electron Spectrum between 5 and
    ~ 300 GeV, unpublished thesis, University of Leiden, 1971

Webber, W. R. and J. M Rockstroh, Cosmic Ray Electrons With E>1GeV-Some
    New Measurements and Interpretations, in press, J. Geophys. Res.,
    1972

15

PMT

PMT

PMT

50 cm

6.4 mm PLASTIC
SCINTILLATOR

12.7 mm UVT LUCITE
CERENKOV COUNTER

LUCITE LIGHT
PIPE

HEIGHT
IN CM
17.3

S1

PMT

SC 1
SC 2

SC 3
SC 4

30 cm

0

DIFFUSION
CHAMBER

6.4 mm PLASTIC SCINTILLATOR

3mm CsI(Na)

S2

-13.5

PMT

PMT

PMT

3mm TUNGSTEN

6.4mm PLASTIC

-36.1

PMT

P. M.

P. M.

P. M.

P. M.

P. M.

6.4 mm PLASTIC
SCINTILLATOR

P. M.

27 mm IRON

P. M.

-108

IONIZATION   SPECTROMETER

1b

ENERGY DISTRIBUTION OF 18-GeV SLAC ELECTRONS

FRACTION OF INCIDENT PARTICLES

ENERGY (GeV)

30%

20%

10%

17

STARTING POINT DISTRIBUTION OF 16-GeV SLAC ELECTRONS

18
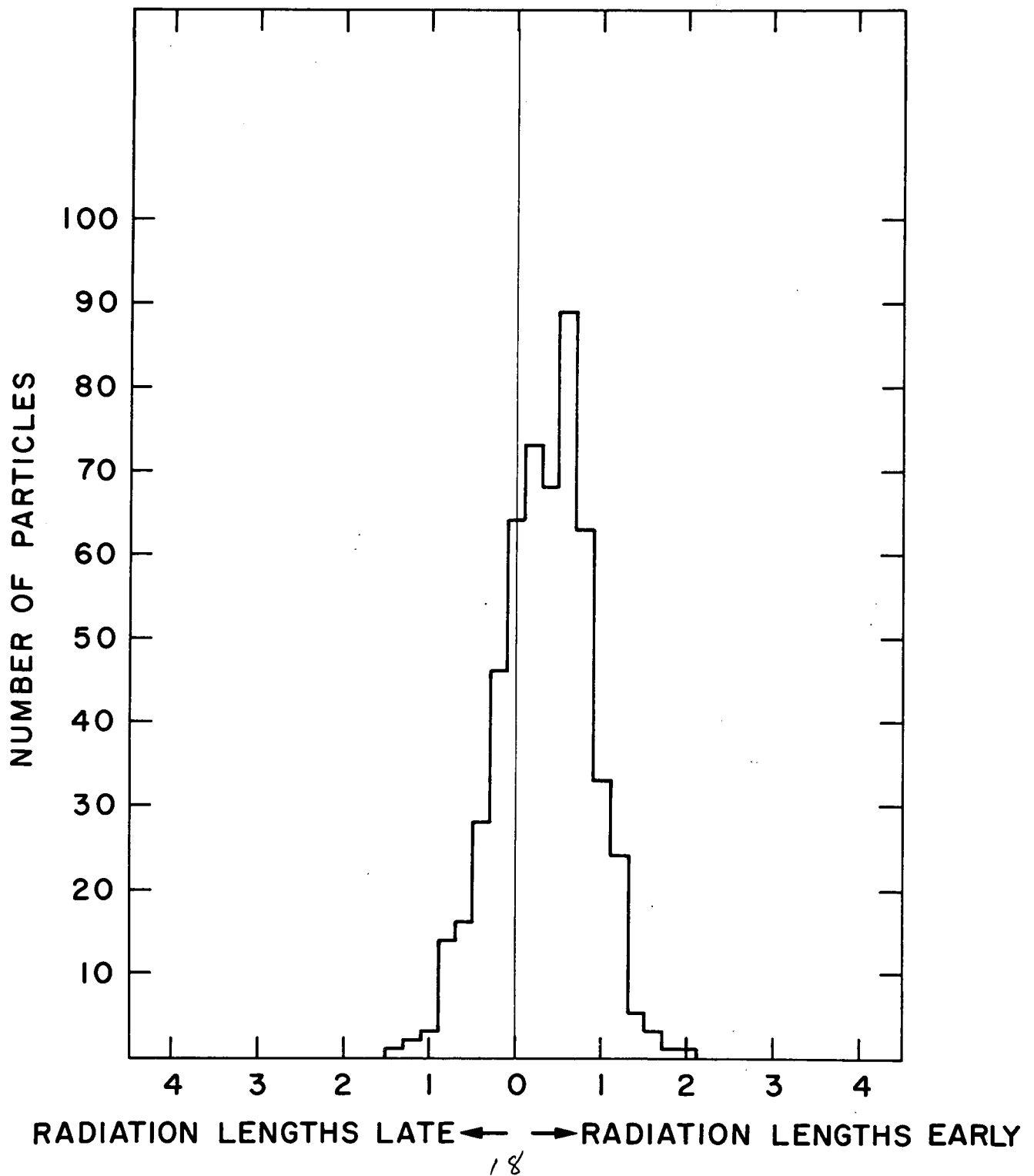
STARTING POINT DISTRIBUTION OF

FLIGHT 3 SINGLE PARTICLES DEPOSITING ≥ 40-GeV IN IRON & ≥ 5-GeV IN TUNGSTEN

(ARROWS INDICATE POSITIONS OF SCINTILLATORS)

DEPTH IN RADIATION LENGTHS FROM 1st TUNGSTEN MODULE

NO. OF EVENTS

20

Y-axis: $\frac{dN}{dE} \times E^3 \left(\frac{(ELECTRONS \ (GeV)^2)}{M^2 - STER - SEC} \right)$

X-axis: ENERGY IN GeV

Legend:
○ FLIGHT 1
● FLIGHT 3
--- BEST POWER LAW FIT
— BEST TRANSITION REGION FIT

21